Korean J. Chem. Eng., 33(3), 823-830 (2016)
DOI: 10.1007/s11814-015-0239-z

pISSN: 0256-1115
eISSN: 1975-7220

Influence of phosphorous addition on $Bi_3Mo_2Fe_1$ oxide catalysts for the oxidative dehydrogenation of 1-butene

Jung-Hyun Park* **and Chae-Ho Shin****,†**

*Division of Physical Science and Engineering, KAUST Catalysis Center (KCC), King Abdullah University of Science and Technology (KAUST), 4700 KAUST, Thuwal 23955-6900, Saudi Arabia
**Department of Chemical Engineering, Chungbuk National University, Chungbuk 28644, Korea
(*Received 15 July 2015 • accepted 11 November 2015*)

Abstract−$Bi_3Mo_2Fe_1P_x$ oxide catalysts were prepared by a co-precipitation method and the influence of phosphorous content on the catalytic performance in the oxidative dehydrogenation of 1-butene was investigated. The addition of phosphorous up to 0.4 mole ratio to $Bi_3Mo_2Fe_1$ oxide catalyst led to an increase in the catalytic performance; however, a higher phosphorous content (above P=0.4) led to a decrease of conversion. Of the tested catalysts, $Bi_3Mo_2Fe_1P_{0.4}$ oxide catalyst exhibited the highest catalytic performance. Characterization results showed that the catalytic performance was related to the quantity of a π-allylic intermediate, facile desorption behavior of adsorbed intermediates and ability for re-oxidation of catalysts.

Keywords: Butadiene, Oxidative Dehydrogenation, $Bi_3Mo_2Fe_1P_x$ Oxide Catalyst, 1-C_4H_8-temperature-programmed Desorption, Temperature-programmed Re-oxidation

INTRODUCTION

Oxidative dehydrogenation (ODH) of butenes is a promising route for producing 1,3-butadiene (BD), which is an important raw material for the manufacture of styrene butadiene rubber (SBR), poly-butadiene rubber (BR), and acrylonitrile-butadiene-styrene resin (ABS), and demand for it is increasing [1-3]. BD is produced through a multistep reaction process. The first step of ODH of butenes consists of the abstraction of α-hydrogen atom from the butene molecules and formation of an allylic intermediate. Next, if the abstraction of second hydrogen and desorption of H_2O on formed allylic species occur, the BD may be formed [1].

An ODH reaction involves various oxide catalysts such as chrome catalysts [4,5], ferrites [6], vanadium catalysts [7,8], bismuth-molybdate based catalysts, etc [9-14]. In particular, bismuth-molybdate based catalysts and multicomponent bismuth-molybdate catalysts are the most intensively studied. In the Bi-Mo catalytic system, Bi-sites are responsible for the catalytic activity, while Mo-sites are related to the selectivity [15]. It is generally known that multicomponent bismuth-molybdate catalysts can be formed as a Mo-Bi-M(II)-M(III)-O catalyst containing divalent metal (M(II)), trivalent metal (M(III)), bismuth, and molybdenum [9,12-17]. To make an excellent bismuth-molybdate based catalyst, it is critical to activate the bismuth via both the divalent and trivalent metal cations. Among the various M(II) or M(III) transition metals, iron is regarded as the most promising component [2,18-20]. The incorporation of iron into a Bi-Mo catalyst helps the transport of oxygen in the catalyst. The role of iron can be seen as enhancing the electron transport in the catalyst by the presence of a Fe^{2+}/Fe^{3+} redox couple during the ODH reaction [2].

Multiple phases exist in the multicomponent bismuth-molybdate catalyst system. Catalysts prepared with different transition metals show the M(II)MoO_4 and Me(III)$(MoO_4)_3$ structure due to the partial replacement of Fe by added metals [2,21]. The role of each phase in the catalytic performance in the ODH reaction of n-butene needs to be discussed; however, it is very difficult to verify their roles in the catalytic performance due to their structural complexity. A few reports have tried to elucidate the roles of each phase. Qiu et al. [22,23] investigated the synergism effect on the catalytic performance in the ODH of n-butene over the $ZnFe_2O_4$ catalyst mechanically mixed with $BiPO_4$, Sb_2O_4, and SnO_2. They suggested that the added oxides played the role of oxygen donor to the active center on the mixed oxides the via redox mechanism.

Phosphate-based catalysts have been studied from the viewpoint of practical applications in commercial processes. A few results have been published about the catalysts, characterization, and their performance in the ODH reaction. Takita et al. [17] reported that the incorporation of phosphorous in metal oxides had stabilized lattice oxygen ions, which are strongly bonded with phosphorous ions. Ai [25] reported that the acid-base property and catalytic performance in the ODH of 1-butene on the Fe_2O_3 catalyst are influenced by the quantity of phosphorous loadings. The addition of small amount of phosphorous promotes the reaction to higher selectivity, resulting from it inhibiting the formation of CO_x products [26,27] in the ODH of iso-butane. Furthermore, phosphorous component has been reported as a promising promoter for the improvement of catalytic stability [16,28].

In this regard, we investigated the influence of phosphorous component for the ODH of 1-butene to 1,3-butadiene (BD) over the $Bi_3Mo_2Fe_1$ oxide catalyst of the main phase of Bi-Mo-Fe oxide cat-

†To whom correspondence should be addressed.
E-mail: chshin@chungbuk.ac.kr

alytic system [9]. Phosphorous-modified $Bi_3Mo_2Fe_1$ oxide catalysts were prepared by a co-precipitation method with varying phosphorous content, and ODH of 1-butene was carried out. The physical properties of the catalysts were characterized by X-ray diffraction (XRD), N_2 sorption and Raman analysis. In addition, to describe the correlation between the catalytic performance and the phosphorous contents on the $Bi_3Mo_2Fe_1P_x$ oxide catalysts, an investigation was conducted using temperature-programmed desorption of 1-butene (1-C_4H_8-TPD) and re-oxidation (TPRO).

EXPERIMENTAL

1. Catalyst Preparation

All chemicals were analytical grade and used as received without further purification. Bismuth molybdate iron oxide catalysts were prepared with a Bi/Mo/Fe/P ratio of 3/2/1/0-1.0 by using co-precipitation method. Typically, for the $Bi_3Mo_2Fe_1P_{0.4}$ oxide catalyst, 16.50 g $Bi(NO_3)_3{\cdot}5H_2O$ (Junsei, 98%) and 4.65 g $Fe(NO_3)_3{\cdot}9H_2O$ (Samchun, 98%) were dissolved in 80 ml de-ionized water that had been acidified with 10% nitric acid (solution A). Solution A was added dropwise into a solution containing 3.96 g $(NH_4)_6Mo_7O_{24}{\cdot}4H_2O$ (Junsei, 99%) under vigorous stirring at 60 °C, and then 0.51 g H_3PO_4 (Samchun, 85%) was added. The pH was adjusted to 5 using NH_4OH (Samchun, 28-30 vol%). The mixed solution was vigorously stirred at 60 °C for 3 h and subsequently removed by using a rotary evaporator (EYELA N-1000). The obtained precipitate was dried at 100 °C for 12 h and calcined at 550 °C for 2 h in flowing air. The catalysts are denoted as $BiMoFeP_x$, where x refers to the molar ratio of phosphorous in the catalyst (x=0.0-1.0).

2. Characterization

The crystallite structure of the $Bi_3Mo_2Fe_1P_x$ oxide catalysts was recorded on an X-ray diffractometer (Bruker D5005) using Ni-filtered CuKα radiation (30 kV and 50 mA) with a scan rate of 1.2° min^{-1}. The Raman spectra were collected with Nexus FT-Raman spectrometer. The spectra were recorded at room temperature using the 1,064 nm line of Nd-YAG laser for excitation. The laser was operated at 0.7 W and the wavenumbers obtained from spectra are accurate to within 2 cm^{-1}. The Brunauer-Emmett-Teller (BET) surface areas and pore volumes of the catalysts were determined from multipoint isotherms (Micromeritics ASAP 2020) using N_2 adsorption at −196 °C. Prior to the measurement, the 0.5 g sample was degassed at 250 °C for 4 h. Elemental analysis was performed by inductively coupled plasma and atomic emission spectroscopy (ICP-AES), using a Jarrell-Ash Polyscan 61E spectrometer, in combination with a Perkin-Elmer 5000 atomic absorption spectrophotometer.

To investigate the adsorption/desorption behavior of the 1-C_4H_8, temperature-programmed desorption of 1-butene (1-C_4H_8 TPD) was performed in a U-shaped quartz reactor. The catalysts were pretreated under a He flow (50 $cm^3{\cdot}min^{-1}$) at 300 °C for 1 h and then cooled to room temperature under the same atmosphere. Each catalyst was then kept in a flow of 1-C_4H_8 (20 $cm^3{\cdot}min^{-1}$) for 0.5 h at room temperature and subsequently, was flushed for 0.5 h with a 20 $cm^3{\cdot}min^{-1}$ He flow to remove physisorbed 1-C_4H_8. After the flushing, the catalyst was heated to 800 °C from room temperature at a rate of 10 °C·min^{-1} and was maintained at 800 °C for 0.5 h to complete desorption of the 1-C_4H_8. The mass signals of *m/z*=44 (·CO_2), 54 (·C_4H_6), and 56 (·1-C_4H_8) in the outlet gas were detected by a mass spectrometer (MS, Balzer QMS 200, Pfeiffer vacuum).

Temperature-programmed re-oxidation (TPRO) was carried out using the same apparatus as that used for TPD of 1-C_4H_8 to elucidate the re-oxidation property of the catalysts. Prior to the analysis, the 0.2 g samples were pretreated at 550 °C for 1 h with a 5% H_2/Ar (50 $cm^3{\cdot}min^{-1}$) flow and then cooled to room temperature. The flow of 5% O_2/N_2 (20 $cm^3{\cdot}min^{-1}$) was then switched into the reactor and, subsequently, the catalyst was heated to 800 °C from room temperature with heating rate of 10 °C·min^{-1}. The mass signal of *m/z*=32 (·O_2) in the outlet gas was measured by using the same MS analyzer as in the TPRO experiments.

Pulse experiments were performed at 420 °C by using the fixed bed reactor. Each 0.1 g catalyst was placed in the U-shaped quartz reactor with densely packed quartz wool. All catalysts were pretreated at 500 °C for 1 h under He flow (50 cm^3 min^{-1}) and subsequently cooled to 420 °C. The pulses were repeated ten times with 9 min intervals. The pulse experiments were carried out by contacting fixed amounts of reactant gases with a He as a carrier gas. Each pulse contained 41 μmole of 1-C_4H_8 and 30 μmole of O_2, respectively. The mass signals of *m/z*=32 (·O_2), 44 (·CO_2), and 54 (·C_4H_6) were detected using the same MS analyzer as that used in the TPRO experiments.

3. Catalytic Performance Test

The ODH of 1-butene was conducted at an ambient pressure with 0.5 g of catalysts in a continuous flow fixed-bed reactor. Prior to the reaction, catalysts were pretreated at 500 °C for 2 h with a 50 cm^3 min^{-1} N_2 flow and cooled to 420 °C under the same atmosphere. The feed composition was fixed at 1-butene/air/steam=1/3.75/5 with a total flow rate of 78 cm^3 min^{-1}. The water was injected into the catalyst bed by a diaphragm liquid dosing pump (KNF, Stepdos 03) and was sufficiently vaporized by passing through an evaporator. Products were analyzed by on-line gas chromatograph

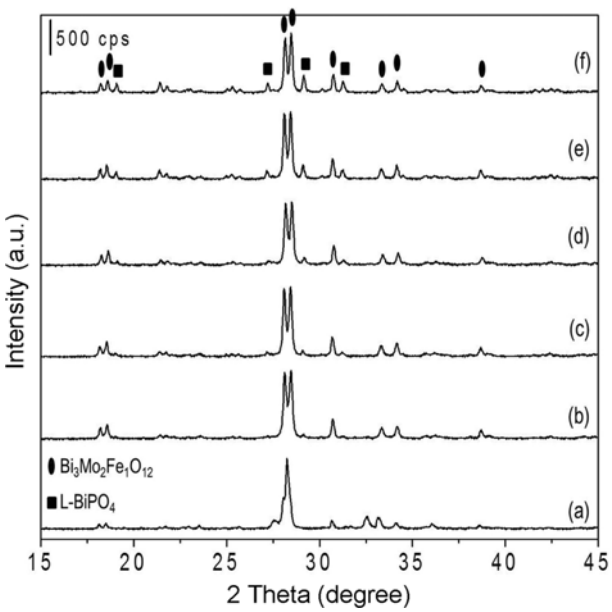

Fig. 1. XRD patterns of the $Bi_3Mo_2Fe_1P_x$ oxide catalysts: (a) $Bi_3Mo_2Fe_1$, (b) x=0.2, (c) 0.4, (d) 0.6, (e) 0.8, and (f) 1.0.

Table 1. Effect of phosphorous contents on structural properties of $Bi_3Mo_2Fe_1P_x$ oxide catalysts

Catalyst	S_{BET} ($m^2\ g^{-1}$)	Pore volume ($cm^3\ g^{-1}$)	Phase conc. (%)[a]		Catalyst composition (mole)[c]			
			$Bi_3Mo_2Fe_1O_{12}$	L-$BiPO_4$[b]	Bi	Mo	Fe	P
$Bi_3Mo_2Fe_1$	4.9	0.019	100	-	2.95	1.97	1.00	-
$Bi_3Mo_2Fe_1P_{0.2}$	2.9	0.005	93.7	6.3	2.94	1.96	1.00	0.20
$Bi_3Mo_2Fe_1P_{0.4}$	2.7	0.007	89.5	10.5	2.95	1.97	1.00	0.40
$Bi_3Mo_2Fe_1P_{0.6}$	3.6	0.005	88.6	11.4	2.93	1.97	1.00	0.56
$Bi_3Mo_2Fe_1P_{0.8}$	2.5	0.009	72.2	27.8	2.92	1.96	1.00	0.76
$Bi_3Mo_2Fe_1P_{1.0}$	3.0	0.004	63.6	36.4	2.95	1.97	1.00	0.95

[a]Calculated from XRD analysis
[b]Low temperature $BiPO_4$ phase
[c]Determined from ICP-AES analysis

(Varian 3800) equipped with flame ionization detector (FID) with an Al_2O_3/KCL column for hydrocarbons and thermal conductivity detector (TCD) with a Porapak Q packed column for CO and CO_2. The conversion, selectivity, and yield of BD were calculated following previously reported procedures [9].

RESULTS AND DISCUSSION

1. Characterizations

To identify the crystallite structure of $BiMoFeP_x$ oxide catalysts, XRD analysis was performed for the catalysts prepared with varying phosphorous content, as shown in Fig. 1 and Table 1. All catalysts were observed mainly the $Bi_3Mo_2Fe_1O_{12}$ phase (2θ=28.1, 28.4 and 31.8°) with a minor phase of a low-temperature $BiPO_4$ (L-$BiPO_4$, 2θ=27.2, 29.2 and 32.5°). $Bi_3Mo_2Fe_1O_{12}$ phase was gradually decreased with increasing phosphorous content, while, L-$BiPO_4$ phase increased (Table 1); it was increased up to 36%, equal to P=1.0 mole ratio. To investigate the phase change before and after the ODH reaction, XRD analysis was also conducted after a 14 h reaction; however, there was no significant change of XRD patterns, except the transformation to a high-temperature $BiPO_4$ phase from L-$BiPO_4$ phase.

The BET surface areas and element analysis of the $BiMoFeP_x$ oxide catalysts are listed in Table 1. Phosphorous-free BiMoFe oxide catalyst possesses a BET surface area of 4.9 $m^2\ g^{-1}$. The BET surface area of $BiMoFeP_x$ oxide catalysts somewhat decreased with the addition of phosphorous and it exhibited values ranging from 2.5 to 3.6 $m^2\ g^{-1}$ without a distinct difference. The molar ratio of each component of the $BiMoFeP_x$ oxide catalysts was similar to the description of the nominal composition of those catalysts.

Raman analysis was conducted to investigate the catalyst structure (Fig. 2). Raman spectrum of bulk $Fe_2(MoO_4)_3$ possesses bands at 992, 968, 825, 783, and 350 cm^{-1}. The bands at 968 and 992 cm^{-1} are the Mo=O symmetric stretches of the three distinct, isolated MoO_4 sites in bulk $Fe_2(MoO_4)_3$ [29,30]. The Raman bands at 783 and 825 m^{-1} are the associated asymmetric stretches of MoO_4 units and the broader band at 350 cm^{-1} is the related bending mode [29, 30]. Note that the weak bands at 992 and 825 cm^{-1} are associated with the $Fe_2(MoO_4)_3$ phase and are not related to the bulk MoO_3 phase. In addition, between the 400 and 600 cm^{-1} region are modes representing BiO bands [31,32]; however, this band is too small and too difficult to distinguish. $Bi_3Mo_2Fe_1O_{12}$ possesses bands at 870, 783, 350 and 285 cm^{-1}, those peaks overlap with the $Fe_2(MoO_4)_3$ peaks, and are in good agreement with literature data [33]. In addition, no evidence for crystalline Fe_2O_3, P_2O_5 and $BiPO_4$ is contained in the Raman spectra. Raman results were also in line with our previous literature data [34]. XRD, Raman, and ICP-AES analysis demonstrated that the $BiMoFeP_x$ oxide catalysts were successfully prepared with varying phosphorous contents.

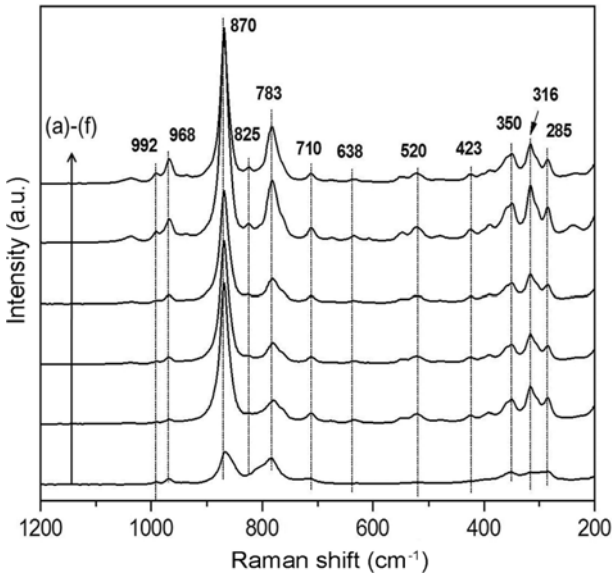

Fig. 2. Raman spectra of the $Bi_3Mo_2Fe_1P_x$ oxide catalyst: (a) $Bi_3Mo_2Fe_1$, (b) x=0.2, (c) 0.4, (d) 0.6, (e) 0.8, and (f) 1.0.

2. Catalytic Performance Test

Fig. 3 shows the catalytic performance of $BiMoFeP_x$ oxide catalysts with respect to the phosphorous content in the ODH reaction of 1-butene to BD after a 14 h reaction, plotted as a function of the phosphorous contents. The main reaction products were by dehydrogenation of 1-butene; and the production of CO and cracking products such as CH_4, C_2H_4, C_2H_6, C_3H_6 and C_3H_8 were negligible in these reaction conditions. For all catalysts, the conversion was stably maintained without a deactivation during the reaction. Conversion of 1-butene increased gradually with increasing the phosphorous content by preventing the combustion reaction, and

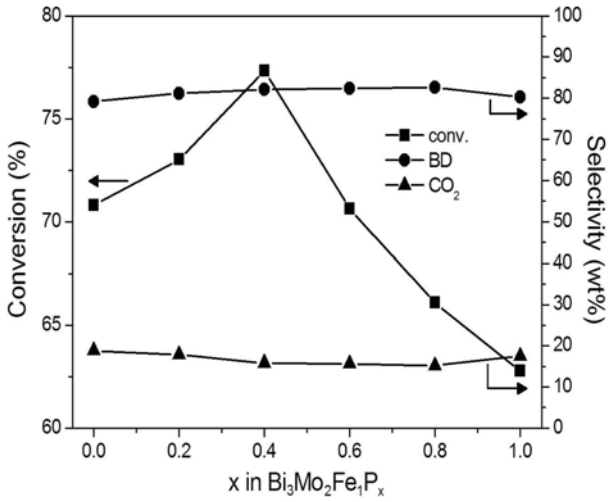

Fig. 3. Catalytic performance of the $Bi_3Mo_2Fe_1P_x$ oxide catalyst in the ODH of 1-butene at 420 °C after a 14 h reaction, plotted as a function of phosphorous content. Reaction conditions: T=420 °C, 0.5 g catalyst, 1-C_4H_8/air/steam=1/3.75/5, and total flow rate=78 cm^3 min^{-1}.

reached a maximum at P=0.4 mole ratio, showing volcano-type conversion profiles. Yield in BD also showed a similar tendency regarding the conversion of 1-butene. The BD selectivity slightly increased with respect to the phosphorous contents, whereas the selectivity to CO_2 decreased; however, there was no distinct difference of selectivity to BD and CO_2 with varying phosphorous content. Of the tested catalysts, the $BiMoFeP_{0.4}$ oxide catalyst exhibits the highest catalytic performance in the ODH of 1-butene. Conversion of 1-butene and the yields in BD on this catalyst were found to be 77.3% and 63.5%, respectively.

3. TPD of 1-C_4H_8 and TPRO

To elucidate the adsorption and desorption behavior of 1-C_4H_8, TPD profiles were made and are shown in Fig. 4. The adsorbed 1-C_4H_8 (*m/z*=56) gradually decreased with increasing the temperature until 450 °C, and above this temperature no further desorption of 1-C_4H_8 was observed, indicating that the 1-C_4H_8 species were completely desorbed. BD (*m/z*=54), H_2O (*m/z*=18) and CO_2 (*m/z*=44) were observed via reaction between adsorbed 1-C_4H_8 and lattice or bulk oxygen species of the catalysts during the TPD analysis (not shown) [9]. The mass signal of BD of product by reaction of 1-butene with lattice oxygen in the catalyst constituted several peaks in all catalysts, indicating the existence of a diverse interaction between 1-C_4H_8 and lattice oxygen in the oxide catalyst. The observed peaks are classified as those weakly and strongly bounded intermediates [35]; one peak is associated with the weakly adsorbed BD species in the temperature range of 70-220 °C, and the other peak is the strongly adsorbed BD species in the range from 300-800 °C. The peak temperature in the weakly bounded BD species shifted to a low temperature with increasing the phosphorous content, indicating that desorption strength of this peak was weakened by the addition of phosphorous. For strongly bounded BD species, the peak of the catalysts that contained small amount of phosphorous (up to P=0.4) shifted to a low temperature compared to the phosphorous-free BiMoFe oxide catalyst, and catalysts that

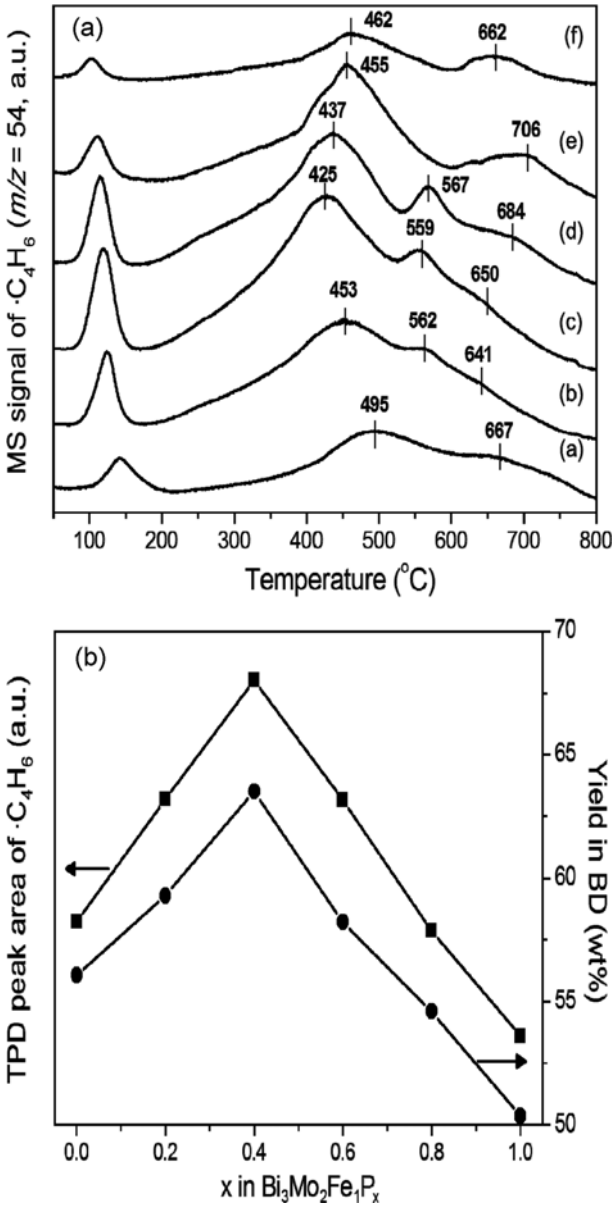

Fig. 4. (A) 1-Butene-TPD profiles of the $Bi_3Mo_2Fe_1P_x$ oxide catalysts and (B) correlation between peak area of BD observed below 220 °C and yield in BD: (a) $Bi_3Mo_2Fe_1$, (b) x=0.2, (c) 0.4, (d) 0.6, (e) 0.8, and (f) 1.0.

contained a high phosphorous content (above P=0.4) shifted to a high temperature. The weak intermediates mean the surface π-allylic intermediate and are responsible for the catalytic performance in the ODH reaction [35]. As mentioned, the formation degree of a π-allylic intermediate through the activation of butenes is an important step in the ODH of 1-butene. The quantity of weakly bounded BD species could be calculated by integrating of TPD peak of below at 220 °C. The quantity of weakly bounded BD species decreased in the following order: $BiMoFeP_{0.4}$>$BiMoFeP_{0.2}$>$BiMoFeP_{0.6}$>BiMoFe >$BiMoFeP_{0.8}$>$BiMoFeP_{1.0}$ (Fig. 4(B)). In addition, the desorption temperature of strongly bounded BD species exhibited a reverse tendency of the quantity of weakly bounded BD species. These results are in good agreement with the catalytic performance of these cat-

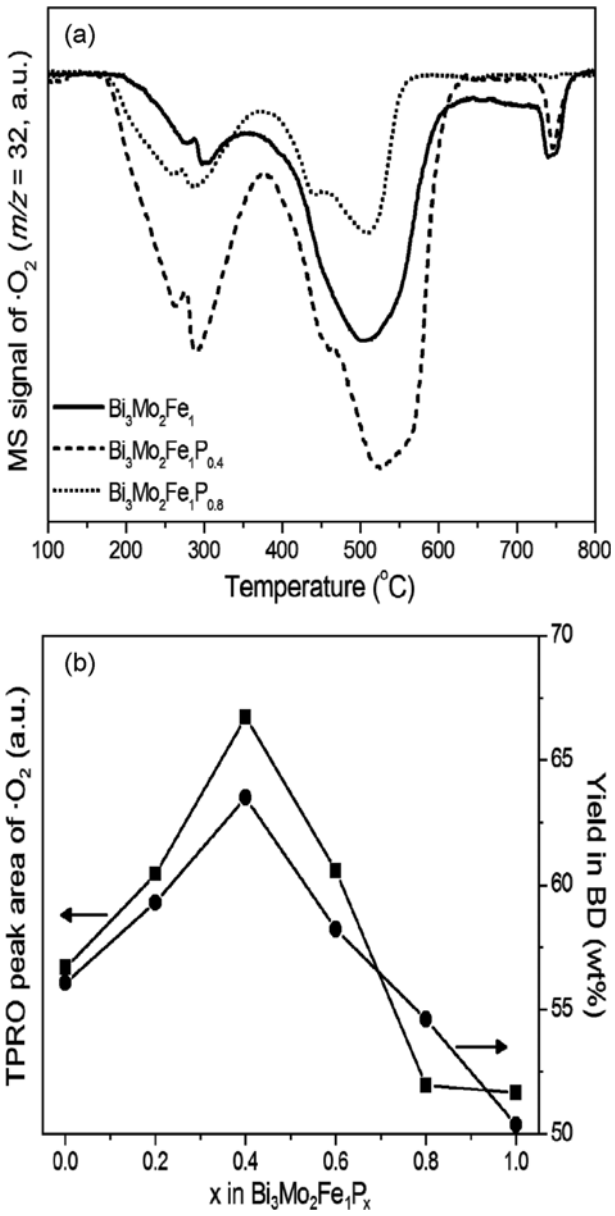

Fig. 5. (A) TPRO profiles of the $Bi_3Mo_2Fe_1P_x$ oxide catalysts and (B) correlation between peak area of O_2 and yield in BD: (a) $Bi_3Mo_2Fe_1$, (b) x=0.2, (c) 0.4, (d) 0.6, (e) 0.8, and (f) 1.0.

alysts. Thus, it can be concluded that the catalytic performance of $BiMoFeP_x$ oxide catalysts is related to the quantity of π-allylic intermediate and facile desorption of BD species.

TPRO analysis was performed over catalyst pretreated by 1-C_4H_8 gas and the results are shown in Fig. 5. Several kinds of peaks were observed for each catalyst (Fig. 5(A)). The first peaks in the 50-380 °C range show two peaks centered at 262 and 280 °C, and the second peaks in the 400-700 °C range show them centered at 525 °C, including two broad shoulder peaks (455 and 568 °C). The first peak of TPRO profiles is assigned to the oxidation of the reduced bismuth oxide. The second peak of TPRO profiles is assigned to the oxidation of the molybdenum oxide [36]. The consumption of molecular oxygen at the first oxidation increased with added phosphorous content, whereas the second oxidation step increased up to P=0.4 mole and decreased above that value. In Bi-Mo based catalyst, bismuth ions (low temperature oxidation) are associated with the catalytic performance and the molybdate ions (high temperature oxidation) with the selectivity of products [37,38]. The relative area obtained by integrating the first oxidation step of TPRO curve means the ability for oxidation of the catalyst. The obtained peak area decreased in the following order: $BiMoFeP_{0.4}$>$BiMoFeP_{0.2}$>$BiMoFeP_{0.6}$>BiMoFe>$BiMoFeP_{0.8}$>$BiMoFeP_{1.0}$ (Fig. 5(B)), and was in good agreement with order of the catalytic performance on these catalysts. Woo et al. reported similar results over Ca-Bi-Mo oxide catalyst in the ammoxidation of propane to acrylonitrile [39]. Unlike with the catalytic performance, there was no clear correlation between the BD selectivity and the tendency of a high temperature oxidation. From what has been shown with the TPRO profiles, it could be concluded that the catalytic performance was attributed to the ability for oxidation of the catalysts.

4. Effect of Reactants on the Catalytic Performance of $Bi_3Mo_2Fe_1P_{0.4}$ Oxide Catalyst

It is well known that the catalytic performance of *n*-butenes shows decreasing tendency according the sequence of 1-butene>*cis*-2-butene>*trans*-2-butene [40] due to their structure [41]. In order to determine the effect of reactant composition for ODH reaction over $BiFeMoP_{0.4}$ oxide catalyst, the ODH reaction with varying reactant composition was performed and the results are in Fig. 6. The used reactant composition is shown in Table 2. The results show that the catalytic performance of $BiMoFeP_{0.4}$ oxide catalyst was strongly dependent on the reactant composition. Conversion obtained with pure 1-butene (77.3%) as a reactant was much higher than that obtained with pure 2-butenes (21.9%) and the mixture of 1-butene and 2-butenes (69.4%). In addition, yield in BD followed the same

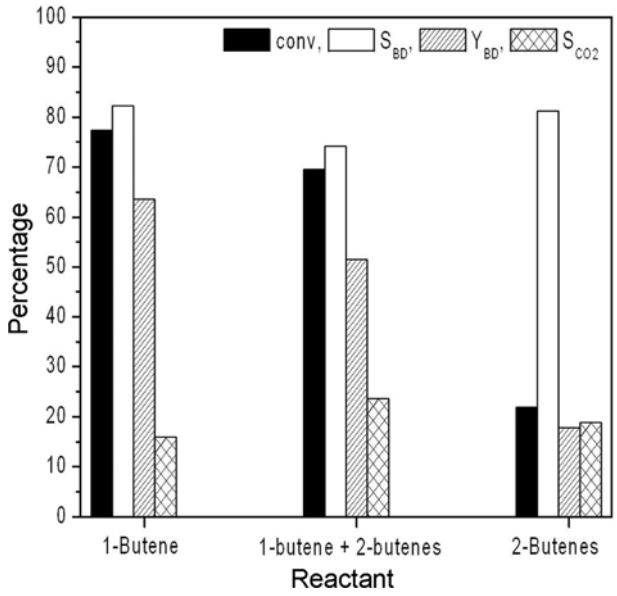

Fig. 6. Effect of reactant composition of the catalytic performance in ODH reaction on the $Bi_3Mo_2Fe_1P_{0.4}$ oxide catalyst, plotted as a function of reactant composition. Reaction conditions: T=420 °C, 0.5 g catalyst, butenes/air/steam=1/3.75/5, and total flow rate=78 cm^3 min^{-1}.

Table 2. Feed compositions employed for the ODH reaction over $Bi_3Mo_2Fe_1P_{0.4}$ oxide catalyst

Reactant	Component (%)			
	1-Butene	*trans*-2-Butene	*cis*-2-Butene	Others
1-Butene	99.3	0.1	0.1	0.5
Mixture (1-butene+2-butenes)	59.0	24.8	15.0	0.2
2-Butenes	0.0	62.0	37.4	0.6

tendency with that of conversion. This result means that 1-butene is more favorable than 2-butenes in the ODH over the $BiMoFeP_x$ oxide catalytic system.

To characterize the differences between 1-butene and 2-butenes in reactivity, TPD experiments of different reactants were performed and are shown in Fig. 7. Both TPD spectra are characteristic of mainly two types of intermediates interactions: One form is released as the product of partial oxidation (BD), and the other form is released as CO_2. This result indicates that the oxygen species in the $BiMoFeP_{0.4}$ oxide catalyst directly reacted with adsorbed butenes to form BD and CO_2. Both selective and nonselective oxygen species are present on the Pd-Fe catalyst in the ODH reaction [42]. Thus, we believe that the formation of BD, and CO_2 was involved in selective and nonselective oxygen species, respectively. The peak area of BD and CO_2 of TPD profiles means the quantity of selective or nonselective oxygen species, respectively. The peak area of BD obtained after 1-butene adsorption is larger than that of after adsorption of 2-butenes, which means that the 1-butene facilitates the reaction with selective oxygen species on the catalyst than that of 2-butenes. In addition, desorption of BD after adsorption 1-butene started at a low temperature of 70 °C, while, it started at 320 °C after 2-butenes adsorption. Thus, the 2-butenes are more strongly adsorbed on the catalyst surface compared to that of 1-butene. This phenomenon can be explained by the site isolation effect: the ODH is favored for 1-butene, but isomerization is promoted for 2-butenes [43]. These results strongly support the conclusion that 1-butene is more favorable than 2-butene in the ODH reaction.

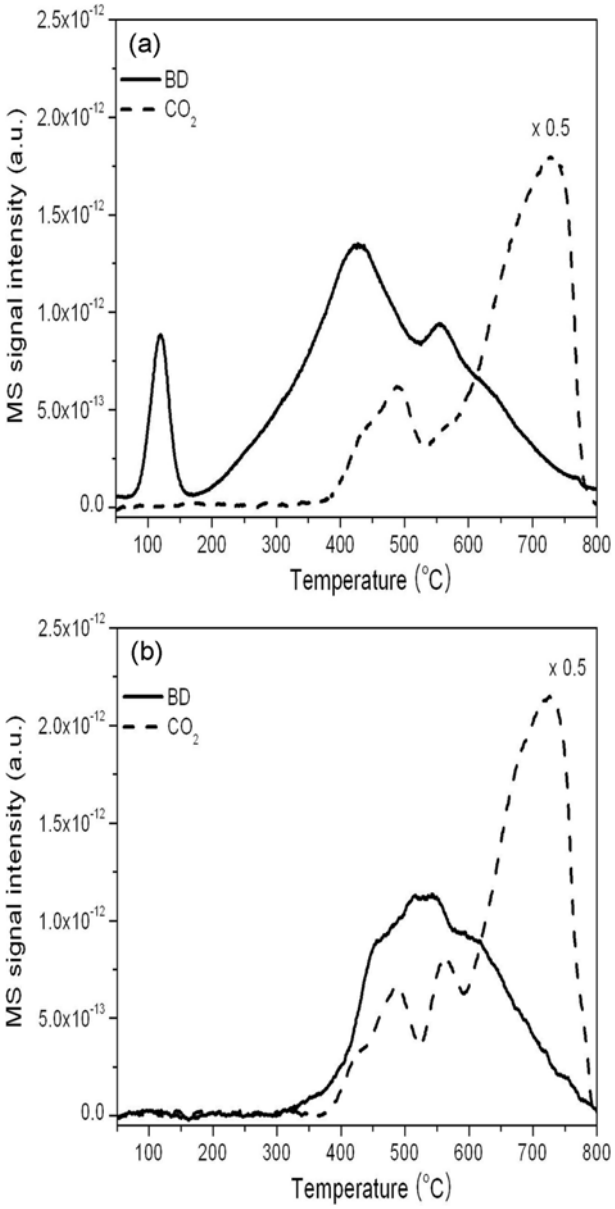

Fig. 7. (a) TPD profiles of 1-butene and (b) 2-butenes over $Bi_3Mo_2Fe_1P_{0.4}$ oxide catalysts.

For CO_2 formation, several kinds of nonselective oxygen species were observed in all TPD profiles. And a distinct peak was detected in the 2-butene-TPD profiles in the temperature range of between 400 °C and 800 °C. The peak area of CO_2 observed in the 2-butene-TPD profile was much larger than that of 1-butene-TPD profile. This result indicates that the 2-butenes are more favorable than 1-butene with nonselective oxygen species of the $BiMoFeP_{0.4}$ oxide catalyst.

5. Effect of the $BiPO_4$ Phase in the ODH Reaction

From the results obtained from the XRD analysis (Table 1), the following basic statements can be made. All $BiMoFeP_x$ oxide catalysts were observed multiphasic, including the $Bi_3Mo_2Fe_1O_{12}$ and $BiPO_4$ phases. The ODH reaction for the $BiMoFeP_x$ oxide catalysts demonstrated that the optimum composition of $Bi_3Mo_2Fe_1O_{12}$ and the $BiPO_4$ phase were presented and strongly affected the catalytic performance. The pure $BiPO_4$ phase revealed very low catalytic performance ($X_{C_4H_8}$=2.6% and S_{BD}=82.7%). In our catalyst system, the $BiMoFeP_{0.4}$ oxide catalyst, which contains a 10% $BiPO_4$ phase, showed higher catalytic performance compared to that of $BiPO_4$-free BiMoFe oxide catalyst. However, the catalytic performance was not completely correlated with the $BiPO_4$ concentration. We therefore may ask, what is the role of the $BiPO_4$ phase in the $BiMoFeP_x$ catalysts? We investigated the role of the $BiPO_4$ phase in the $BiMoFeP_x$ oxide catalysts.

To verify the effect of the $BiPO_4$ phase, biphasic catalysts were

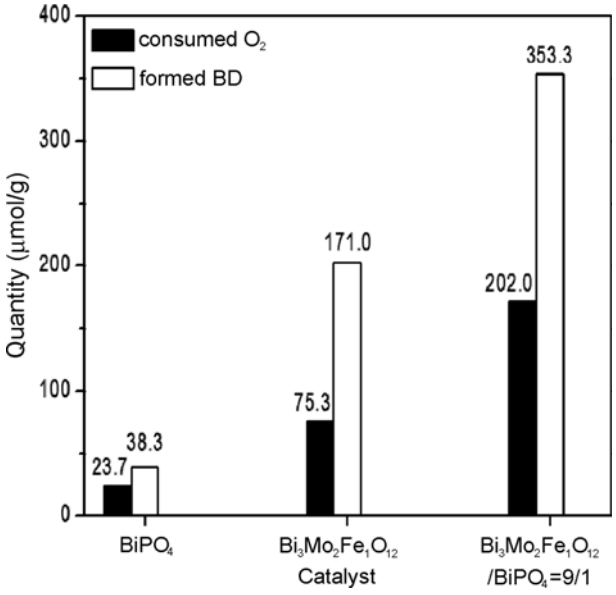

Fig. 8. BD formation profiles obtained during the O_2 and 1-C_4H_8 pulse experiments for catalysts of $BiPO_4$, $Bi_3Mo_2Fe_1O_{12}$, and $Bi_3Mo_2Fe_1O_{12}$/$BiPO_4$=9/1 which was mechanically mixed in weight. Pulse experiments were repeated 10 times with 9 min intervals at 420 °C.

prepared by mildly mixing separately prepared $Bi_3Mo_2Fe_1O_{12}$ and L-$BiPO_4$ in proportions of R_m=0.9. R_m means that the phase concentration of $BiMoFeP_{0.4}$ oxide catalyst obtained from XRD analysis. The composition of the mixtures of $Bi_3Mo_2Fe_1O_{12}$ and L-$BiPO_4$ was expressed as the mass ratio:

$$R_m = \frac{\text{weight of } Bi_3Mo_2Fe_1O_{12}}{\text{weight of } Bi_3Mo_2Fe_1O_{12} + \text{weight of L-}BiPO_4}$$

To make a mixed oxide (BiMoFe+BiP), hexane was used as a solvent and treated by using ultrasonic waves to mix for 0.5 h. After that, the hexane was removed by using a rotary evaporator and dried at 100 °C for 12 h. The catalyst was used without further heat treatment. Fig. 8 shows the BD formation profiles observed during the pulse experiments. Contacting catalysts with 1-C_4H_8 and O_2 resulted in the simultaneous formation of CO_2 and C_4H_6, which are the products of 1-C_4H_8 with lattice or surface oxygen species. Comparing the quantity of CO_2 with BD, the quantity of CO_2 was much larger than that of BD, indicating that the complete oxidation reaction was more favored than the selective oxidation reaction during the pulse experiments (not shown). Here, we focused the O_2 consumption and BD formation obtained by reaction between 1-C_4H_8 and selective oxygen species. The quantity of the consumed O_2 and formed BD was calculated by integrating each peak, and the total quantity of those was shown. The total quantity of consumed O_2 and formed BD of the mixed BiMoFe+BiP oxide catalyst was much larger than that of the two oxide catalysts and decreased in the following order: BiMoFe+BiP>BiMoFe>BiP. This result led to the conclusion that the O_2 consumption and BD formation were promoted in the presence of $BiPO_4$ phase. This synergy effect can be explained by the remote control mechanism: one phase, the donor, dissociates gas phase oxygen to surface mobile species, which spills over to the other phase, the acceptor [1,2]. The acceptor is regarded as the potentially active phase. In our catalytic system, the $Bi_3Mo_2Fe_1$ oxide catalyst can be seen an acceptor phase and $BiPO_4$ is the donor phase. Therefore, the $BiPO_4$ phase plays a role as an oxygen donor and leads to the enhancement of the catalytic performance.

CONCLUSIONS

Phosphorous modified $Bi_3Mo_2Fe_1$ oxide catalysts were prepared by a co-precipitation method and the ODH of 1-butene to BD was carried out. The catalytic performance and physicochemical properties of $Bi_3Mo_2Fe_1P_x$ oxide catalyst were influenced by the phosphorous content. Of the tested catalysts, the $Bi_3Mo_2Fe_1P_{0.4}$ oxide catalyst showed the highest catalytic performance and a volcano-type curve with respect to the phosphorous content. Combined with the 1-C_4H_8-TPD and TPRO results it is concluded that the catalytic performance was related to the quantity of a π-allylic intermediate and the ability for oxidation of the catalysts. Small amount of $BiPO_4$ phase in the $Bi_3Mo_2Fe_1$ oxide catalyst led to the enhancement of the catalytic performance as an oxygen donor. In this catalyst system, 1-butene was more favorable than 2-butene in the ODH reaction.

ACKNOWLEDGEMENT

This work was supported by the Energy Efficiency and Resources of the Korea Institute of Energy Technology Evaluation and Planning (KETEP) granted financial resource from the Ministry of Trade, Industry and Energy, Republic of Korea (No. 2014021194).

REFERENCES

1. G. Ertl, H. Knozinger and J. Weitkamp, in: Handbook of Heterogeneous Catalysis, VCH, Weinheim, 2253 (1997).
2. L. T. Weng and B. Delmon, *Appl. Catal. A: Gen.*, **81**, 141 (1992).
3. W. C. White, *Chemico-Biological Interactions*, **166**, 10 (2007).
4. J. A. Pena, A. Monzon and J. Santamaria, *J. Catal.*, **142**, 59 (1993).
5. A. Brito, R. Arvelo, R. Villarroel, F. J. Garcia and M. T. Garcia, *Chem. Eng. Sci.*, **51**, 4385 (1996).
6. H. H. Kung and M. C. Kung, *Adv. Catal.*, **33**, 159 (1985).
7. S. De Rossi, M. Lo Jacono, M. Gardini and P. Porta, *J. Catal.*, **146**, 126 (1994).
8. J.-H. Park and C.-H. Shin, *Appl. Catal. A: Gen.*, **495**, 1 (2015).
9. J.-H. Park, H. R. Noh, J. W. Park, K. H. Row, K. D. Jung and C.-H. Shin, *Appl. Catal. A: Gen.*, **431-432**, 137 (2012).
10. J.-H. Park, K. H. Row and C.-H. Shin, *Catal. Commun.*, **31**, 76 (2013).
11. J.-H. Park, H. R. Noh, J. W. Park, K. H. Row, K. D. Jung and C.-H. Shin, *Res. Chem. Intermed.*, **37**, 1125 (2011).
12. Y. Moro-Oka and W. Ueda, *Adv. Catal.*, **40**, 233 (1994).
13. H. W. Lee, J. C. Jung, S. H. Kim, Y. M. Chung, T. J. Kim, S. J. Lee, S. H. Oh, Y. S. Kim and I. K. Song, *Korean J. Chem. Eng.*, **26**, 994 (2009).
14. J. C. Jung, H. W. Lee, S. Y. Park, Y. M. Chung, T. J. Kim, S. J. Lee, S. H. Oh, Y. S. Kim and I. K. Song, *Korean J. Chem. Eng.*, **25**, 1316 (2008).

15. T.-J. Park, *Oxidative dehydrogenation of butenes over zinc ferrite catalysts*, Ph. D Thesis, Rice Univ. (1987).
16. G. J. Nolan, US Patent, 3,320,329 (1967).
17. Y. Takita, X. Qing, A. Takami, H. Nishiguchi and K. Nagaoka, *Appl. Catal. A: Gen.*, **296**, 63 (2005).
18. J. F. Brazdil, D. D. Suresh and R. K. Grasselli, *J. Catal.*, **66**, 347 (1980).
19. T. S. R. Prasada Rao and K. R. Krishnamurthy, *J. Catal.*, **95**, 209 (1985).
20. Ph. A. Batist, C. G. M. van de Moesdijk, I. Matsuura and G. C. A. Schuit, *J. Catal.*, **20**, 40 (1971).
21. M. W. J. Wolfs and P. H. A. Batist, *J. Catal.*, **32**, 25 (1974).
22. F.-Y. Qui, L.-T. Weng, P. Ruiz and B. Delmon, *Appl. Catal.*, **47**, 115 (1989).
23. F.-Y. Qiu, L.-T. Weng, E. Sham, P. Ruiz and B. Delmon, *Appl. Catal.*, **51**, 235 (1989).
24. F. H. Hoppstock, US Patent, 4,002,696 (1977).
25. M. Ai, *J. Catal.*, **60**, 306 (1979).
26. I.-C. Marcu, M. N. Urlan, A. Rédey and I. Săndulescu, *C. R. Chimie*, **13**, 365 (2010).
27. V. Schwartz, H. Xie, H. M. Meyer, S. H. Overbury and C. Liang, *Carbon*, **49**, 659 (2011).
28. Y. M. Chung, Y. T. Kwon, T. J. Kim, S. J. Lee and S. H. Oh, *Catal. Lett.*, **131**, 579 (2009).
29. H. F. Christmann, US Patent, 3,270,080 (1966).
30. L. E. Briand, A. M. Hirt and I. E. Wachs, *J. Catal.*, **202**, 268 (2002).
31. H. Tian and L. E. Wachs, *J. Phys. Chem. B.*, **109**, 23491 (2005).
32. I. Matsuura, R. Schut and K. Hirakawa, *J. Catal.*, **63**, 152 (1980).
33. W. M. Sears and W. J. Keeler, *Appl. Spectrosc.*, **46**, 1898 (1992).
34. S. A. Veniaminov and G. B. Barannik, *React. Kinet. Catal. Lett.*, **13**, 413 (1980).
35. H. Miura, Y. Morikawa and T. Shirasaki, *J. Catal.*, **39**, 22 (1975).
36. R. K. Grasselli, J. D. Burrington, D. J. Buttrey, Jr. P. DeSanto, C. G. Lugmair, Jr. A. F. Volpe and T. Weingand, *Top. Catal.*, **23**, 5 (2003).
37. T. Uda, T. T. Lin and G. W. Keulks, *J. Catal.*, **62**, 26 (1980).
38. S. I. Woo, J. S. Kim and H. K. Jun, *J. Phys. Chem. B*, **108**, 8941 (2004).
39. H. H. Voge and C. R. Adams, *Adv. Catal.*, **17**, 151 (1967).
40. A. N. Vasilev and P. N. Galicia, *Chem. Technol. Fuels Oils*, **33**, 185 (1997).
41. S. E. Golunski and A. P. Walker, *J. Catal.*, **204**, 209 (2001).
42. M. F. Portela, *Top. Catal.*, **15**, 241 (2001).